JOURNAL OF MATERIALS SCIENCE 25 (1990) 2025–2035

Transformation yielding, plasticity and crack-growth-resistance (R-curve) behaviour of CeO_2–TZP

CHENG-SHENG YU, D. K. SHETTY
Department of Materials Science and Engineering, University of Utah, Salt Lake City, Utah 84112, USA

Transformation yield and plasticity, transformation zone sizes at crack tips and rising crack-growth-resistance (R-curve) behaviours were studied in a commercial-grade ceria partially stabilized zirconia polycrystalline material (CeO_2–TZP). The yield stresses measured in three-point bending decreased from 390 to 176 MPa when the sintering temperature was varied from 1425 to 1525° C. The corresponding total plastic strain to fracture increased with decreasing yield stress. Crack-tip transformation zones in precracked, annealed and loaded single-edge-notch-bend specimens decreased significantly in size with increasing transformation yield stress; however, the R-curves were relatively insensitive to the yield stresses or the transformation zone sizes. The measured zone sizes and R-curves were examined in terms of both crack shielding and plastic yield strip zone models.

1. Introduction

Crack shielding models [1–3] have been successfully used to explain many aspects of transformation toughening in MgO–partially stabilized zirconia (MgO–PSZ), Y_2O_3–partially stabilized zirconia (Y_2O_3–TZP) and zirconia-toughened alumina ceramics. Thus, for example, the rising crack-growth-resistance (R-curve) measured in MgO–PSZ by Swain and Hannink [4] and Marshall and Swain [5] is qualitatively consistent with the R-curve behaviour predicted by the crack shielding models due to the transformation wake behind the advancing crack tip. Further, Swain [6] and Swain and Rose [7] have successfully correlated the saturation fracture toughness of MgO–PSZ and Y_2O_3–TZP with the square root of the widths of the transformation zones in accordance with the crack shielding models. The transformation zone sizes in the above studies were, however, measured indirectly on fracture surfaces using X-ray diffraction techniques [8, 9], because the zones are not sufficiently well defined for observation in optical or scanning electron microscopes.

Recent development of certain grades of ceria–partially stabilized zirconia (CeO_2–TZP) ceramics that exhibit pronounced transformation plasticity has permitted direct observation of the shapes and sizes of the transformation zones in precracked fracture mechanics test specimens [10, 11]. A quantitative comparison of the observed shapes and sizes of the transformation zones and the measured R-curve behaviour with the theoretical predictions by Yu and Shetty [10] revealed several interesting anomalies in CeO_2–TZP. First, the transformation zone was elongated in the plane of the crack, i.e. the zone length ahead of the crack was much greater than the zone width normal to the crack plane. This zone shape was shown to be inconsistent with the prediction of a combined shear/dilatation yield criterion established in macroscopic biaxial tests. Secondly, even though the maximum transformation zone widths measured in CeO_2–TZP ($> 300\,\mu m$) were more than an order of magnitude larger than the transformation zone widths in MgO–PSZ ($\sim 25\,\mu m$), the maximum fracture toughness measured in the two materials were comparable ($K_c \sim 14$ to 15 MPa $m^{1/2}$). Finally, both the transformation zone sizes and the R-curves measured with precracked and annealed single-edge-notch-bend (SENB) specimens of CeO_2–TZP did not show evidence of saturation, i.e. both the transformation zone dimensions and the crack-growth-resistance were increasing up to the point of instability.

The present paper summarizes the results of an investigation in which the transformation yield stress of a CeO_2–TZP was systematically varied by varying the sintering temperature. The objective was to examine the effect of the varying yield stress on transformation plasticity, the crack-tip transformation zone size and the R-curve behaviour in the context of crack shielding and plastic strip zone models.

2. Test material and procedures

The CeO_2–TZP ceramic used in the present study was obtained in powder form from a commerical source (tentative grade Z-65, Ceramatec Inc., Salt Lake City, Utah 84119, USA). Nominally, it is partially-stabilized zirconia with 12 mol% CeO_2 and small amounts of proprietary additives. The as-received powder was first sieved through a 70 μm screen. The

0022–2461/90 $03.00 + .12

TABLE I Sintering temperatures, average grain sizes, phase contents and yield stresses for CeO_2–TZP specimens

Type	Sintering temperature (°C)	Grain size (μm)	Phase content (as-annealed) V_T (%)	Yield stress (MPa)	Phase content (fracture surface) V_T (%)
IA	1500	1.91	98	190	15
IIAA	1525	2.18	98	176	15
IIA	1500	1.87	98	245	18
IIB	1475	1.73	99	281	19
IIC	1450	1.52	99	335	22
IID	1425	1.47	99	390	27

screened powder was pressed in a uniaxial die press at 34.5 MPa, followed by isostatic pressing at 207 MPa. The as-pressed compacts were sintered in air at temperatures ranging from 1425 to 1525° C for 2 h. Test specimens were from two powder lots I and II and were sintered at five different temperatures: 1525° C (type AA), 1500° C (type A), 1475° C (type B), 1450° C (type C) and 1425° C (type D); these are listed in Table I along with the corresponding average grain sizes, phase contents (volume per cent of the tetragonal phase) and yield stresses measured in three-point bend tests. The CeO_2–TZP powders of lots I and II differed slightly in their composition and this was reflected in the different grain sizes and properties of specimens of types IA and IIA, even though these specimens were sintered at the same temperature. The grain sizes were determined by intercept length measurements on scanning electron micrographs of polished and thermally etched surfaces. Approximately 700 grain intercept lengths were measured for each material to obtain the average grain size and the grain size distribution. The tetragonal phase contents were measured by X-ray diffraction using the calibration reported by Toraya *et al.* [12].

Transformation yielding and plasticity were characterized in three-point bending using beam specimens measuring 4 mm × 5 mm × 45 mm in dimensions and a 40 mm span. The test fixtures conformed to the specifications of the MIL standard [13]. The specimens were machined from the sintered billets by cutting with diamond blades and grinding with diamond wheels. The tensile surface was successively polished with 15, 6 and 1 μm diamond paste to achieve a surface that was adequate for surface observations of transformation plasticity. All machined and polished specimens were annealed at 1000° C for 30 min in air prior to the bend tests. There was no detectable change in the phase content after annealing. In selected specimens, strain gauges were mounted in the centre of the tensile surface to monitor the elastic and transformation strains.

Crack-tip transformation zones and crack-growth-resistance curves were studied in prepracked, annealed and reloaded single-edge-notch-bend (SENB) specimens. The relative dimensions of the specimens were according to the specifications of American Society for Testing Materials Standard E 399-83 [14]. The final dimensions of the specimens were support span, $S = 60$ mm, specimen width, $W = 15$ mm, and specimen thickness, $B = 7.5$ mm. This relatively large specimen size was used to meet the minimum size requirements specified in ASTM E 399-83 based on the expected range of fracture toughness and the yield stresses of the material. The SENB specimens were first notched in the centre of the beam to a depth of 1.5 mm using a 150 μm thick diamond blade, loaded in an universal testing machine to precrack to a depth of 3.0 to 3.5 mm ($a/W \sim 0.2$ to 0.25) and subsequently annealed at 1000° C for 30 min. To assess R-curve behaviour, the precracked and annealed SENB specimens were loaded incrementally, unloaded, and the crack lengths (a) and the transformation zone dimensions (zone length, l, and zone width, w) were measured with a stereo microscope and a micrometer stage. The measurements were repeated as a function of applied load and crack length. The transformation zones were photographed at various stages using an optical microscope with Nomarski interference contrast capability.

3. Experimental results and analysis

3.1. Transformation yield, plasticity and failure in three-point bending

Three-point bending was selected over four-point bending previously used [10] because the CeO_2–TZP used in this study deformed in discrete transformation bands normal to the beam axis. In four-point bending, multiple bands nucleated in the centre span and the measured yield stress and the stress–strain curve tended to vary depending upon the number and location of the transformation bands relative to the strain gauge used to monitor the strain. In contrast, a single wedge-shaped transformation band nucleated in three-point bending with a characteristic strain burst and a distinct yield stress associated with the nucleation event. Thus, yield stress could be defined more precisely in three-point bending.

Fig. 1 shows the stress–strain curve obtained in three-point bending for CeO_2–TZP material identified as IIA. The strain plotted was measured at the centre of the tensile surface using a strain gauge. The initial elastic strain rate of the outer fibres during bending was $8.0 \times 10^{-5}\,\text{sec}^{-1}$. The stress was calculated from the load using the conventional elastic bending formula. The stress–strain curve consisted of an initial elastic regime where the stress increased linearly up to a maximum stress which was defined as the yield stress. Yielding commenced with an increment of transformation strain which occurred at the same stress or slightly decreasing stress. This instantaneous strain increment coincided with the formation of the wedge-shaped transformation band at the centre of the bend specimen directly opposite to the loading roller. Fig. 2 shows this transformation band

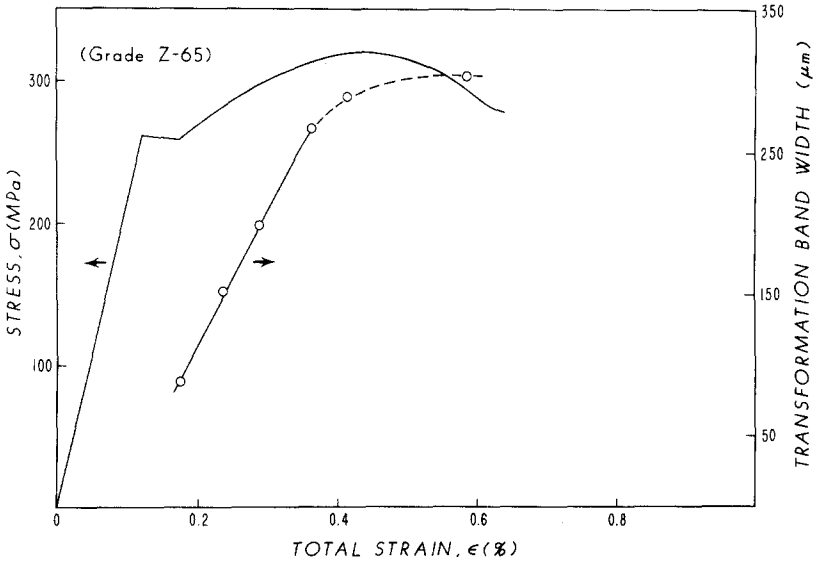

Figure 1 Elastic stress and transformation band width as functions of the measured total strain in three-point bending of CeO_2–TZP (Type IIA).

immediately after nucleation in type IIA CeO_2–TZP. In Fig. 2, the photograph labelled a shows the transformation band on the tension surface, while photograph b shows the wedge shape of the transformation band on the side surface of the beam specimen. The transformation band had the largest width on the tension surface and the width decreased in a direction toward the neutral axis. Reyes-Morel and Chen [15] have reported similar observations of discrete, wedge-shaped transformation bands in four-point bending of CeO_2–TZP. There was no transformation band on the compression side of the bend specimen and this was consistent with the much higher transformation yield stress in compression as compared to the yield stress in tension for CeO_2–TZP as reported previously [10, 15].

Further bending of the beam specimen beyond the yield point increased the surface width and depth of the transformation band. This increase of the width of the transformation band at the centre of the specimen (referred to as the primary band) as a function of the strain is also plotted in Fig. 1. The primary band width increased linearly with strain up to the maximum load corresponding to a nominal stress of about 319 MPa. Figs 3a and b show the primary transformation band at the maximum load. In addition, secondary transformation bands nucleated and grew on either side of the primary band. The stress–strain curve corresponding to the growth of the bands showed a monotonic increase of stress with decreasing work-hardening rate. Typically, in three-point bending, five independent transformation bands were observed to nucleate and grow during the inelastic bending stage.

At the maximum load, a surface crack nucleated within the primary transformation band (see Fig. 4). The surface crack extended stably beyond the maximum load until the final fracture load, which corresponds to unstable fast propagation of the surface crack. The stable growth of the surface crack was a manifestation of a rising crack-growth-resistance behaviour of the CeO_2–TZP. In the regime of surface crack nucleation and growth, the width of the primary transformation band increased much more slowly and appeared to approach a saturation width (see Fig. 1).

3.2. Effect of grain size on transformation yield stress and plasticity

Fig. 5 shows the stress–strain curves corresponding to

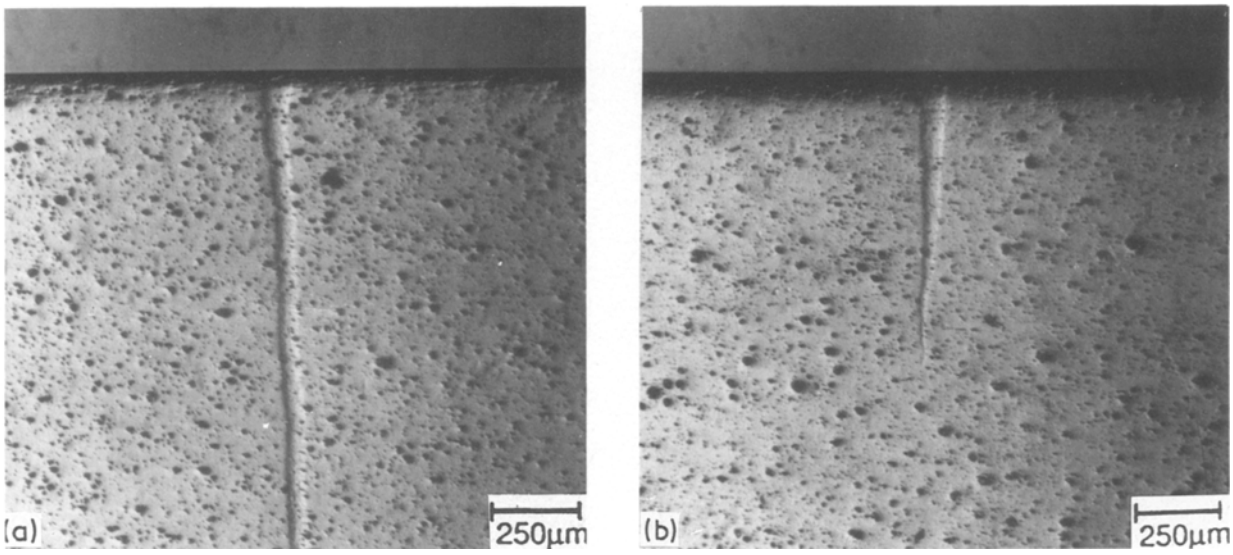

Figure 2 Primary transformation band on (a) the tension surface and (b) on the side surface of a three-point bend specimen of CeO_2 TZP (Type IIA) at yield point (σ_y = 245 MPa).

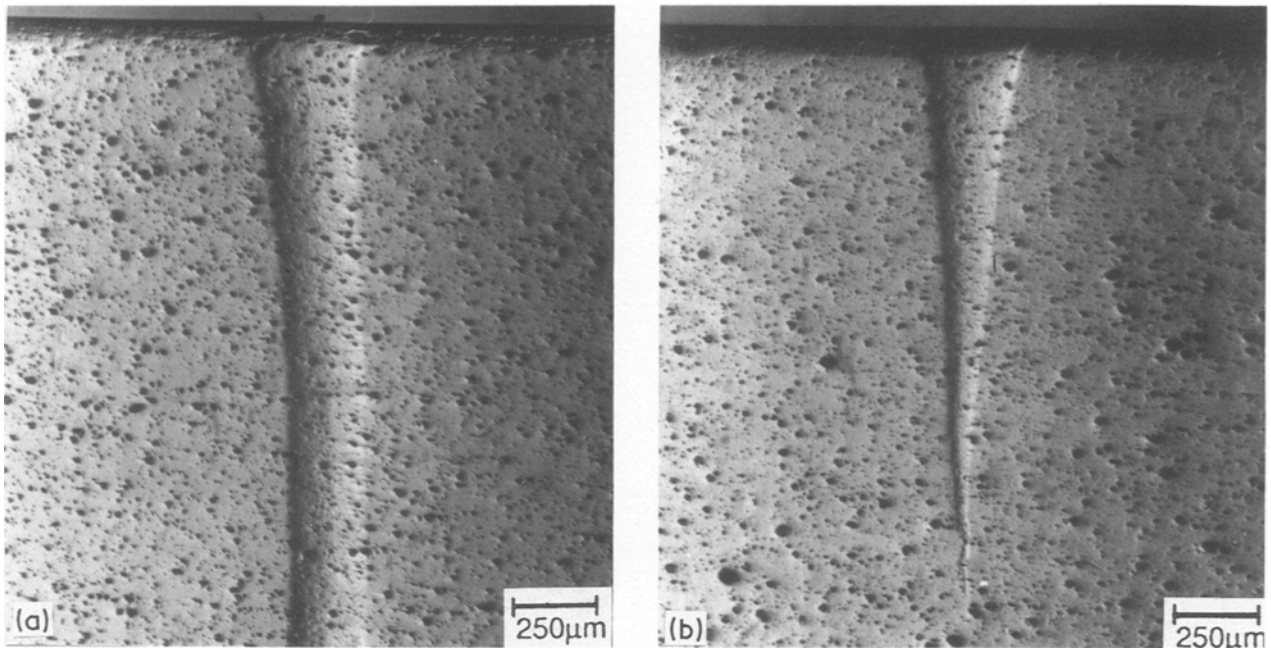

Figure 3 Primary transformation band on (a) the tension surface and (b) on the side surface of the three-point bend specimen of CeO_2TZP (Type IIA) at the maximum stress point (σ = 319 MPa).

the six different types of CeO_2–TZP designated IA, IIAA, IIA, IIB, IIC and IID. The only significant difference among these types was the average grain size (see Table I) and the grain size distribution. Small differences in grain size produced significant differences in both the transformation yield stress and the total strain to fracture. The yield stress increased from 176 to 390 MPa and the total strain to fracture decreased from 1.2% to 0.22% with a decrease in grain size from 2.18 to 1.47 μm. It is intriguing to note that these large differences in the yield stresses and the total strains to fracture occur among the six types despite the fact that volume fractions of the tetragonal phase in both sintered materials and on their fracture surfaces are not very different.

Fig. 6 shows a plot of the transformation yield stress as a function of the average grain size of the zirconia grains. The decrease of the yield stress with increase in the average grain size in Fig. 6 could be adequately described by the following equation

$$\sigma_y = A + \frac{B}{\bar{d}} \quad (1)$$

where σ_y is the yield stress defined as the elastic stress corresponding to the initial transformation burst and $\bar{d}$ is the average grain size. Optimum values for the two constants in the equation determined by regression analysis were $A = -275$ MPa and $B = 952$ MPa μm. Extrapolation based on Equation 1 suggests a critical average grain size of approximately 3.5 μm at which the yield stress would approach zero. The physical basis for choosing the inverse grain size dependence for the transformation yield stress will be discussed in a later section. The compressive yield stress versus the martensitic burst temperature (M_b) correlation established by Reyes-Morel and Chen [15] for different grades of CeO_2–TZP is also a similar manifestation of the grain size influence on transformation yield stress because compositions of the different CeO_2–TZPs were presumably the same.

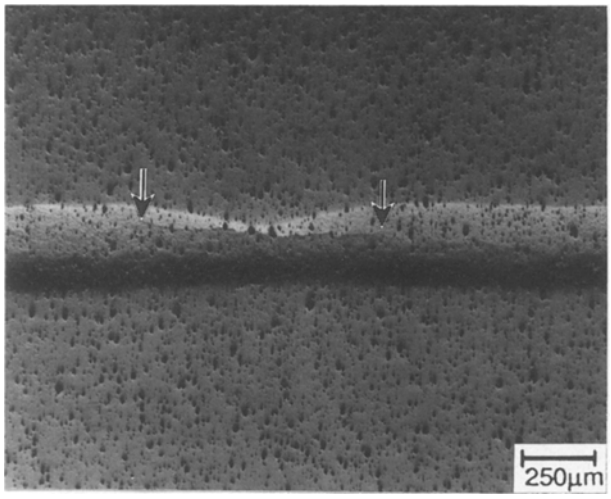

Figure 4 Surface crack within the primary transformation band in the three-point bend specimen of CeO_2TZP (Type IIA).

3.3. Effect of yield stress on crack-tip transformation zone size and crack-growth-resistance behaviour of CeO_2–TZP

Fig. 7 shows plots of the fracture toughness as functions of the normalized crack length, i.e. R-curves, for four types of CeO_2–TZPs. For all the four materials, the R-curves were measured in approximately the same crack-length range, $a/W \sim 0.2$ to 0.35. This relatively short crack length range was used to ensure sufficient elastic ligament length beyond the crack tip and the transformation zone as required by ASTM E-399 [14]. The most noteworthy result in Fig. 7 is that the R-curves for the four different types of CeO_2–TZPs are very similar. A significant amount of the fracture toughness increment was associated with increase in the size of the crack-tip transformation zone without

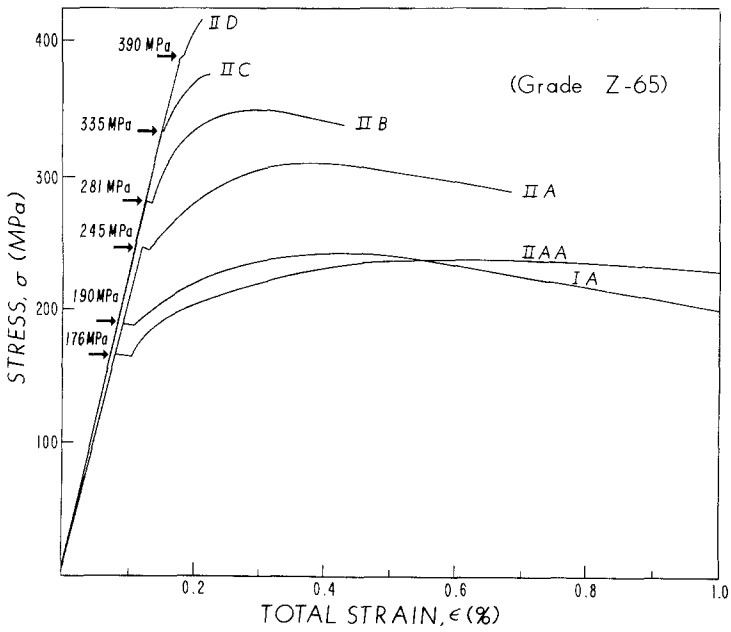

Figure 5 Stress–strain curves for six types of CeO_2TZP obtained in three-point bending.

a concurrent increase in the crack length. Beyond this stationary crack regime, the fracture toughness increased with increasing crack lengths and reached a maximum value in the range 12 to 14 MPa $m^{1/2}$. The R-curve did not show evidence of a saturation fracture toughness; instability set in when the fracture toughness was still increasing.

The similarity of the R-curves was particularly intriguing in view of the fact that crack-tip transformation zone sizes were significantly different for the four different CeO_2–TZP materials. Fig. 8 shows the transformation zones in the different CeO_2–TZPs at an applied stress intensity of 10 MPa $m^{1/2}$. The shapes of the transformation zones were similar, but the relative sizes were very different. Table II summarizes the characteristic dimensions of the transformation zones, length l, and width, w (see Fig. 8e for their definition) for the four materials at different applied stress intensities. The maximum transformation zone width measured for the type IA CeO_2–TZP ($w_{max} \sim 340\,\mu m$) was about seven times the maximum zone width in the type IIC material ($w_{max} \sim 50\,\mu m$). Despite this large difference in the transformation zone widths, the R-curves and the maximum fracture toughness observed for these two CeO_2–TZPs were nearly identical.

3.4. Analysis of the R-curves in terms of crack-shielding models

The major objective of this study was to examine the effect of the varying yield stress on the crack-tip transformation zone size and the R-curve behaviour and compare the results to crack-shielding and plastic strip-zone models. According to the crack-shielding models of transformation toughening, the crack-tip transformation zone width, w, and the extent of

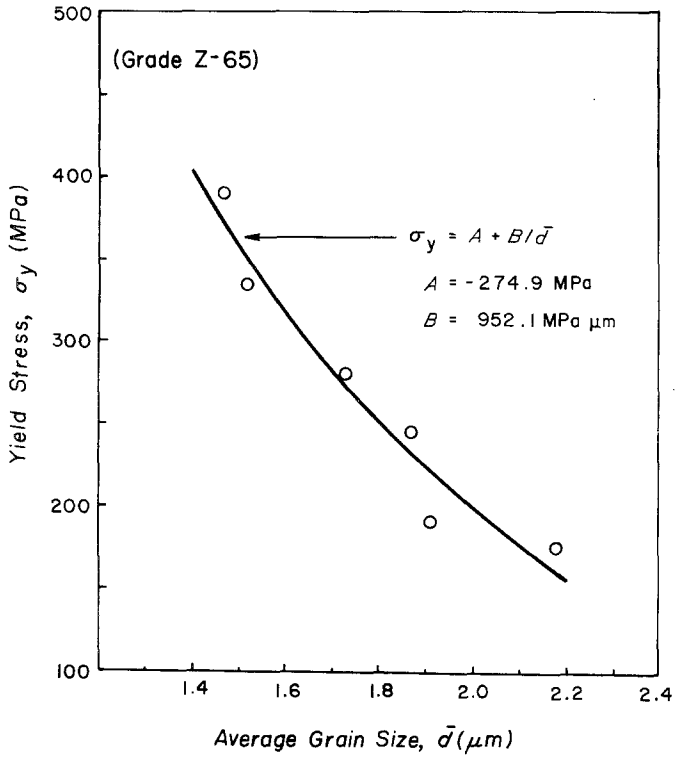

Figure 6 Variation of the transformation yield stress with average grain size for the six different types of CeO_2TZP.

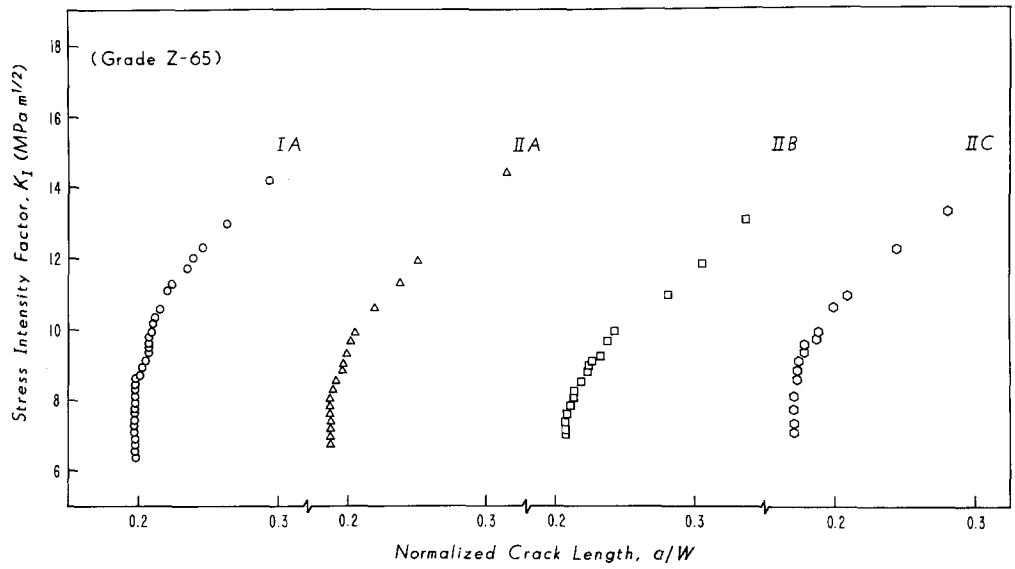

Figure 7 Crack-growth-resistance curves (R-curves) for the four types of CeO_2–TZP assessed in single-edge-notch-bend tests.

crack growth into the transformed zone, Δa, to form a transformation wake behind the crack-tip, are important parameters (among others) that determine the degree of toughening and the R-curve behaviour. The model of McMeeking and Evans [1], for example, gives the following equation for the toughness increment, ΔK_I, as a function of the normalized crack length increment, $\Delta a/w$

$$\Delta K_I = \frac{Ee^T V_f w^{1/2}}{(1 - \nu)} \kappa \left(\frac{\Delta a}{w}, \nu\right) \quad (2)$$

where E is the elastic modulus of the matrix containing the zirconia particles, e^T the transformation strain, V_f the volume fraction of transformed zirconia particles, ν Poisson's ratio, and $\kappa(\Delta a/w, \nu)$ is a function whose value increases with relative crack extension and approaches an asymptotic value at $\Delta a \sim 5w$. The function κ, in effect, describes the R-curve behaviour. The magnitude of the asymptotic value is 0.215 according to the model of McMeeking and Evans [1], who considered only the dilatational component of the transformation strain. Lambropoulos [3] has proposed a model that includes both shear and dilatational strain contributions during nucleation and the predicted asymptotic value for κ in his model is 0.55 $(1 - \nu)$. Swain [6] and Swain and Rose [7] have shown that measurements of the saturation fracture toughness and the zone size in Y_2O_3–TZP and MgO–PSZ ceramics are in good agreement with the above models, respectively.

Fig. 9 compares the R-curves measured for the four types of CeO_2–TZP with the prediction of the crack-shielding model of McMeeking and Evans [1]. To calculate the stress-intensity increment, ΔK_I, from the measured stress intensity at various crack lengths, a baseline fracture toughness, $K_{Ic}^M = 3.0\,\text{MPa m}^{1/2}$, was assumed for the predominantly monoclinic zirconia material in the immediate neighbourhood of the crack tip. In addition, to plot the experimental data in the same form as the theory, the following values were assumed for the constant parameters: $\nu = 0.3$, $E = 200\,\text{GPa}$, $e^T = 0.05$ and $V_f = 0.8$. Of these parameters, only the volume fraction of the transformed tetragonal zirconia in the transformation zone, V_f (assumed to be equal to the difference between the tetragonal contents of the as-sintered ceramic and the fracture surface) is likely to vary among the four types of CeO_2–TZP. The accuracy of the measurements of the tetragonal content, particularly on the fracture surface, was such that no significance could be attached to the small differences observed among the four types of zirconia. For this reason, a common value, $V_f = 0.8$, was used in the comparison in Fig. 9.

Fig. 9 shows that experimentally measured fracture toughness increments from the transformation zones are less than the prediction of the McMeeking and Evans model [1]. Type IA CeO_2–TZP, which exhibited the lowest yield stress and correspondingly the largest transformation zone, showed the maximum deviation from the theory. The fracture toughness of type IIC CeO_2–TZP was closest to the theory, but even here the discrepancy was greater than a factor of 2. In addition to this quantitative difference in the fracture toughness increments, there were several other important

TABLE II Transformation zone dimensions and stable crack extension in single edge notch beam specimens of CeO_2–TZPs

K_I (MPa m$^{1/2}$)	IA			IIA			IIB			IIC		
	w (μm)	l (μm)	Δa (μm)	w (μm)	l (μm)	Δa (μm)	w (μm)	l (μm)	Δa (μm)	w (μm)	l (μm)	Δa (μm)
7.0	41	437	0	19	130	0	19	154	0	11	79	0
8.0	81	897	0	48	486	0	33	328	70	28	221	0
9.0	125	1580	92	66	702	129	46	527	298	33	288	32
9.9	166	1961	181	87	1018	284	53	641	562	49	416	270
13.0	308	3277	1030				56	551	2083	32	305	1697

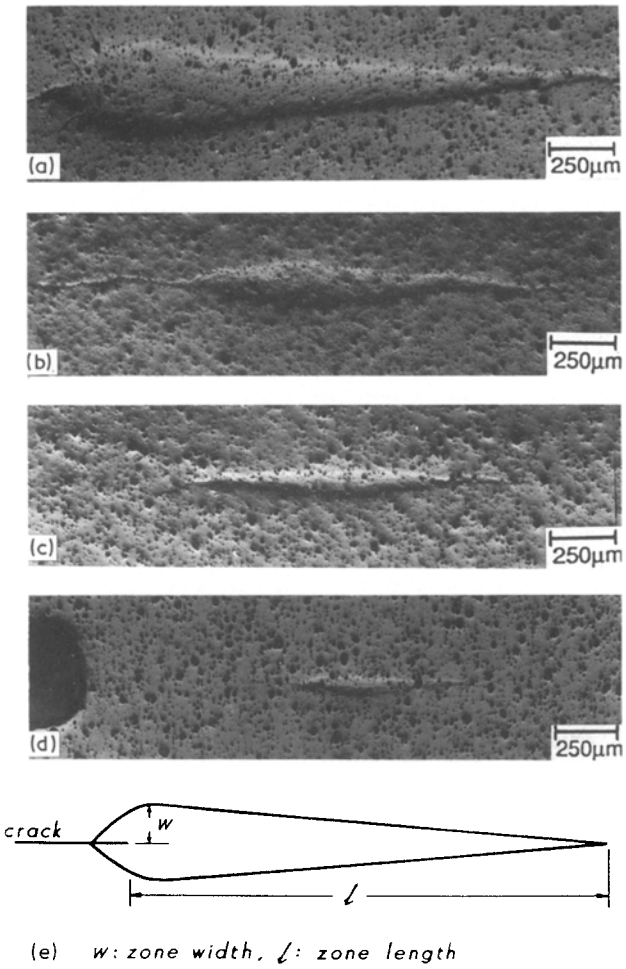

Figure 8 Crack-tip transformation zones in single-edge-notch-bend specimens of the four types of CeO_2TZP at $K_I = 10\,MPa\,m^{1/2}$: (a) type IA, (b) type IIA, (c) type IIB and (d) type IIC. (e) Schematic drawing of the transformation zone used for definition.

differences between the experimental results and the assumptions of the theoretical model. Thus, for example, in the theoretical model all of the fracture toughness increment occurs in conjuction with an increase in the crack length; in other words fracture toughness increase in crack shielding occurs only when the transformation wake builds behind the advancing crack tip. In contrast, experiments indicated that a significant fraction of the fracture toughness increase was associated with stationary crack; i.e. fracture toughness increased with increase in the size of the transformation zone without a concurrent increase in the crack length (see Table II). Secondly, the theory assumes a constant zone width, w, dictated by the transformation yield stress as the crack advances. Experiments indicated that the zone width increased with increasing crack lengths (see Table II), particularly for the low yield stress materials. The zone widths identified in Fig. 9 are the specific values at the indicated crack length increments and they are close to the final values at instability. Finally, in the theory, fracture toughness increment saturates at $\Delta a/w \sim 5$, while the experimental R-curves showed rising fracture toughness up until the point of instability. It is interesting to note in Fig. 9 that the experimental plots of the normalized fracture toughness increments, ΔK_I, show constant plateau values in the entire range of crack lengths. This is a consequence of the fact that fracture toughness of CeO_2–TZP materials typically scale with $w^{1/2}$ during a significant part of the rising R-curve behaviour. Yu and Shetty [10] have shown that this is a general consequence of the growth of the transformation zone of the same shape.

One obvious difference between the experimental results and the theoretical expectation based on fracture mechanics analysis is the shape of the transformation zones at crack tips in CeO_2–TZP materials. Yu and Shetty [10] and Rose and Swain [11] have addressed this issue in detail. The observed transformation zones are thin, elongated strips, while theoretical calculations predict more circular zones. In fact, it is this zone shape which prompted an analysis of the zone length in terms of the plastic strip zone model of Dugdale [16]. In the following paragraphs, transformation zone lengths observed in the four types of CeO_2–TZP are analysed using Dugdale's model.

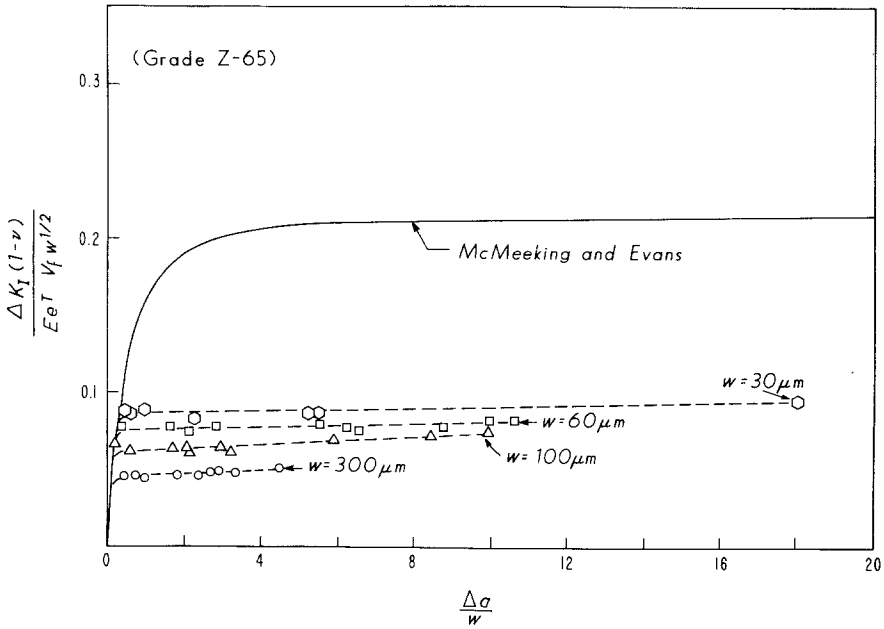

Figure 9 Comparison of R-curves measured for CeO_2–TZPs with the crack-shielding model of McMeeking and Evans [1], using single-edge-notch-bend tests.

3.5. Analysis of the transformation zone lengths in terms of the Dugdale plastic strip zone model

Dugdale [16] assumed that plasticity at a crack tip was concentrated in a strip in front of the crack. Further, the crack of length, a, with the plastic strip zone of length, l, was treated, in effect, as a crack of length $(a + l)$ in which crack closing traction of a magnitude equal to the yield stress was uniformly distributed in the strip zone. Finally, the crack-tip stress singularities from the remote stress and the crack-surface tractions were assumed to cancel to give a finite stress equal to the yield stress at the crack tip [17]. By rewriting the original Dugdale equation, which was developed for a centre-cracked panel under uniform tension, in terms of the elastic stress-intensity factor (assuming small-scale yielding condition prevails) for the single-edge-notch-beam specimen, we get the following equation for the transformation zone length ahead of the crack tip

$$\frac{l}{a + l} = 2 \sin^2 \left[\frac{\pi K_I^{eff}}{4\sigma_y [\pi(a + l)]^{1/2}} \right] \quad (3)$$

In Equation 3, K_I^{eff} is the stress intensity defined in terms of the effective crack length, $(a + l)$ and σ_y is the yield stress measured in uniaxial tension. Plastic zone length measurements in thin sheets of mild steel by Dugdale [16] and in silicon steel by Hahn and Rosenfield [18] have been found to be in agreement with the above model.

Fig. 10 compares the transformation zone length measurements in the single-edge-notch-beam specimens of the four CeO_2–TZPs with the prediction of Equation 3. Transformation zone lengths (l), crack lengths (a) and the effective stress intensity (K_I^{eff}) at different stages of both the stationary (filled points) and the stably-growing crack (open points) were used to construct the experimental plot of Fig. 10. The yield stresses measured in three-point bending were used to normalize the stress-intensity factor on the right-hand side of Equation 3. Fig. 10 shows that the zone length measurements in the CeO_2–TZPs are in good agreement with the Dugdale model.

4. Discussion

An attempt has been made in this study to vary systematically the transformation yield stress and plasticity in a commercial-grade CeO_2–TZP ceramic by varying the sintering temperature and the resulting grain-size distribution. The objective was to study the effect of the varying yield stress on the crack-tip transformation zone sizes, shapes and the R-curve behaviours. More specifically, it was desired to examine quantitatively the dependence of the fracture toughness increments during stable crack growth on the growth and size of the crack-tip transformation zones. Polycrystalline zirconia, partially stabilized with 12 mol % CeO_2, is particularly well-suited for this purpose because transformation zones are readily observed in the material using an optical microscope and Nomarski interference contrast technique.

The trend of increasing yield stress with decreasing grain size observed for CeO_2–TZP in this study is consistent with the essential characteristics of stress-activated transformation plasticity [15]. Below the tetragonal–monoclinic equilibrium temperature, both increasing stress (hydrostatic tension and/or shear) and decreasing temperature promote the transformation of the metastable tetragonal phase to the monoclinic form. Further, as discussed by Heuer *et al.* [19], Garvie and Swain [20] and others (see the review by Evans and Cannon [21]), stability of the (metastable) tetragonal zirconia phase in ceramic matrices increases, i.e. M_s temperature decreases, with decreasing grain size. An inverse linear relationship between the critical grain size and the transformation temperature (M_s) is a natural consequence in an "end-point" energy balance analysis of stability involving volume-dependent energy terms (chemical free energy and strain energy) and surface-area-dependent energy terms (interfacial energy and twin-boundary energy) [20, 21]. Thus, the inverse dependence of the transformation yield stress on the grain size (Fig. 6 and Equation 1) can be viewed as a stress equivalence to the grain-size dependence of the transformation temperature, because the applied stress is introduced in the energy balance in terms of an interaction energy modifying the strain energy term [21]. It is also equivalent to the inverse correlation between the yield stress in compression and the spontaneous martensitic transformation temperature (M_b or M_s) established for

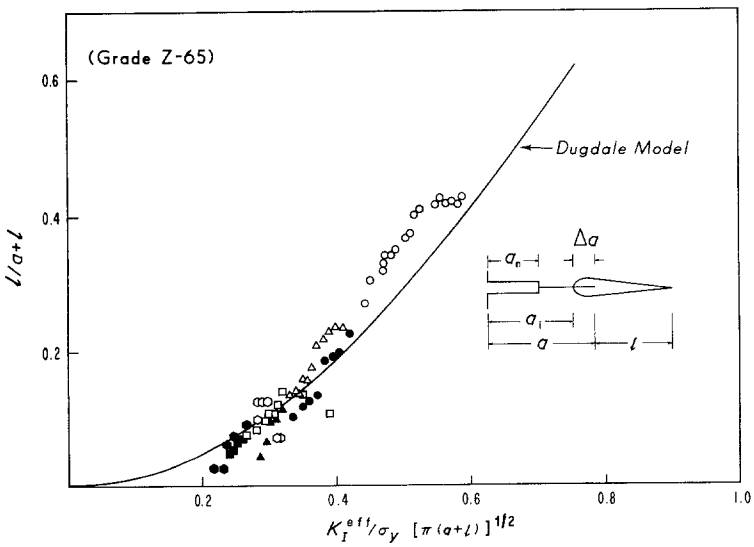

Figure 10 Comparison of the dependence of the transformation zone lengths on the applied stress intensity in CeO_2–TZPs with the Dugdale plastic strip zone model using single-edge-notch-bend tests. (●, ▲, ■, ⬢) Stationary cracks, (○, △, □, ⬡ stably extending cracks. (●, ○) IA, (▲, △) IIA, (■, □) IIB, (⬢, ⬡) IIC.

CeO_2–TZP ceramics by Reyes-Morel and Chen [15] because the M_s temperature is a measure of the stability of the tetragonal zirconia and it decreases with decreasing grain size. In this connection, the critical grain size suggested by Fig. 6 can be interpreted as the grain size of a CeO_2–TZP ceramic for which the M_s temperature is the room temperature. The interrelationship between temperature, applied stress and grain size that defines the condition for transformation has been addressed by many investigators and it has been reviewed recently by Evans and Cannon [21].

The second aspect of the transformation yielding and plasticity of CeO_2–TZP observed in the present study is the discrete nature of the transformation bands analogous to Luders bands in steels. Reyes-Morel and Chen [15] have also observed such localized transformation bands in both compression and bend specimens. From a purely end-point thermodynamics point of view as discussed above, transformation should start with the largest grains in the body and it should extend to smaller and smaller grains with increasing stress. Correspondingly, the stress–strain curve should show a gradual transition from elastic to plastic behaviour and at least in the initial stages of deformation it should be confined to isolated grains. The instantaneous formation of a transformation band of macroscopic dimensions suggests that transformation in CeO_2–TZP is a cooperative phenomenon. Grains adjacent to an already transformed grain are favoured over other isolated grains. Reyes-Morel and Chen [15] attribute this to multiple-site nucleation and call the process autocatalysis. It is interesting to note several aspects of the band formation in three-point bend specimens. Invariably, two bands nucleate at the specimen edges, propagate toward each other rapidly and join to form a single band whose length equals the bend specimen width. Secondly, once nucleated, the band grows much more easily in the depth direction than along the axial direction on the tension surface (see Figs 2 and 3). This result is despite the fact that stress gradient is much more severe in a direction perpendicular to the neutral axis than along a direction parallel to the neutral axis and on the tension surface. First, it was thought that shear stress in the beam, which is zero at the surface and increases toward the neutral axis, was responsible for this elongated zone depth. However, depth of the wedge-shaped zone in the centre span section of four-point bend specimens (where the shear stress is zero) was not significantly different from that in three-point bend specimens. Therefore, reason for the more pronounced growth of the transformation band in the thickness direction is not known.

The most significant result of this study is the relative insensitivity of the crack-growth-resistance curves to the varying yield stress and the size of the crack-tip transformation zones. This has two consequences when we compare the measured fracture toughness increments with the prediction of the crack-shielding model of McMeeking and Evans [1]. First, the fracture toughness increments measured for all the four types of CeO_2–TZP are lower than the predictions of the model (see Fig. 9). Secondly, CeO_2–TZPs with the lower yield stresses (and correspondingly larger transformation zone sizes) show greater deviation from the model prediction than the higher yield stress grades.

In the above comparison, three material parameters, which affect the normalized fracture toughness increment plotted in Fig. 9, are subject to error. These are volume fraction of transformed tetragonal phase, V_f, intrinsic fracture toughness of the transformed zone material, K_{Ic}^M and the transformation zone width, w. The value used for V_f (0.8) was based on X-ray diffraction analyses of the fracture surface and the initial sintered ceramic. The measurement on the fracture surface is subject to an error of at least 10%. In addition, fracture surface measurement gives a measure of V_f in the middle of the transformation zone. It is possible that V_f decreases within the transformation zone at locations away from the fracture surface. If this situation exists in CeO_2–TZP, then, the assumed value for V_f, which should be an average value to correspond with the assumption of the model, would be an overestimate. A smaller average value of V_f would shift the experimental points in Fig. 9 closer to the prediction of McMeeking and Evans [1]. A technique other than X-ray diffraction would be required to assess such local variations in V_f. The ΔK_I values plotted in Fig. 9 were based on an assumed fracture toughness, $K_{Ic}^M = 3\,\text{MPa}\,\text{m}^{1/2}$, for the transformed material in the neighbourhood of the crack tip. This is a conservatively low value and is comparable to the fracture toughness of monoclinic Y_2O_3–TZP [22]. It is unlikely that significant error was introduced in the choice of this value. The measured values of w can be in error if the measurements of the zone width on the specimen surface, where plane stress condition prevails, are not representative of the bulk of the specimens subjected to plane strain condition. To answer this question, a number of single-edge-notch-beam specimens were cut normal to the crack on a plane coinciding with the maximum width of the transformation zone. The as-cut surfaces were gently ground and polished. The transformation zones could be detected on the polished cross-section and the zone widths were found to be essentially uniform through the thickness of the SENB specimens. Thus, surface measurements of zone widths are representative of the bulk of the specimens and error in w is not likely to have caused the discrepancy in Fig. 9.

The similarity of the R-curves for the four different CeO_2–TZPs, despite the differences in their zone sizes, suggests that the transformation zones in the four types of materials do not behave the same way in terms of crack shielding. The larger zones in the lower yield stress materials are counteracted by a secondary factor to obtain a similar degree of crack shielding. Variations in V_f or different degrees of microcracking within the transformation zones are possible candidates for equalizing the crack-shielding effect for different zone sizes.

The agreement obtained between the Dugdale strip zone model and the experimental measurements in Fig. 10 is similar to our earlier result on type

IA material [10]. It is interesting to note that zone lengths in all the four types of CeO_2–TZPs superpose adequately on a single plot close to the prediction of the Dugdale model. The agreement with the Dugdale model is obtained both in the regime of the stationary crack (filled points in Fig. 10) as well as the stably growing crack (open points in Fig. 10). This result is, in one sense, not surprising because the Dugdale model, in essence, postulates a plastic zone in the shape of a thin strip ahead of the crack tip, a situation closely followed by the transformation zone in CeO_2–TZP. In another sense, however, the result is surprising. The original experiments of Dugdale [17] as well as the subsequent studies of Hahn and Rosenfield [19] have shown that in metals the Dugdale model is obeyed in thin sheets where the plastic zones are comparable to the thickness of the sheet. In contrast, the present measurements on CeO_2–TZP were on thick specimens where the specimen thickness was considerably greater than the zone size. It is this question which prompted the query about the possible difference between the transformation zones on the surface and in the bulk.

Although the original Dugdale model accounts for the length of the transformation zones in CeO_2–TZP, it is, in itself, not a substitute for transformation toughening models such as the crack shielding model. However, the Dugdale model can be adapted to include a failure criterion (such as, for example, a critical crack opening displacement) and, thus, model the saturation fracture toughness as has been done by Hahn and Rosenfield [19] and, more recently, Rose and Swain [11]. Such models have not been explicitly developed, however, to explain the rising crack-growth-resistance behaviour.

A final point concerns the R-curve behaviour pertinent to the surface cracks developed within the transformation band in the three-point bend specimens (see Fig. 4). The stable growth of the surface crack following its nucleation suggests a rising crack-growth-resistance. The R-curve behaviour corresponding to the surface crack was assessed by measuring the surface dimension of the crack, $2c$, at different loads during bending. The stress-intensity factor, K_I, for the surface crack was calculated at different stages of the stable growth by assuming a semicircular shape (radius, c) and using the following equation [23]

$$K_I = 2\sigma_b \left(\frac{c}{\pi}\right)^{1/2} F \qquad (4)$$

where σ_b is the bending stress and F is a nondimensional stress-intensity coefficient dependent on the location on the crack front and the size of the crack relative to the beam dimensions. Numerical results for F reported by Newman and Raju [23] were used to calculate stress-intensity factors at both the intersection point of the crack front with tension surface ($\phi = 0$) as well as the deepest point of the crack ($\phi = \pi/2$). The R-curves for the surface crack calculated using Equation 4 at the two crack-front locations are compared with the R-curve measured using the single-edge-notch-beam specimen in Fig. 11. It should be noted that in plotting the R-curve for the single-edge-notch-beam specimen stress-intensity is plotted as a function of the increment crack extension (Δa), while the R-curves for the surface crack are plots of K_I against c, the radius of the surface crack. There are two interesting results in Fig. 11. First, stress-intensity factors for the surface crack are significantly different at the surface point and in the interior. This is due to the assumption of a semicircular shape for the surface crack. When the size of the semicircular crack becomes a significant fraction of the bend specimen size, stress-intensity differences increase as a result of the stress gradient. In reality, crack shape may be closer to a semiellipse than a semicircle. For this case, stress-intensity would be more uniform along the crack front and in between the two extreme cases plotted in Fig. 11.

A second more interesting result in Fig. 11 is the difference between the R-curves for the surface cracks and the R-curve obtained with the single-edge-notch-

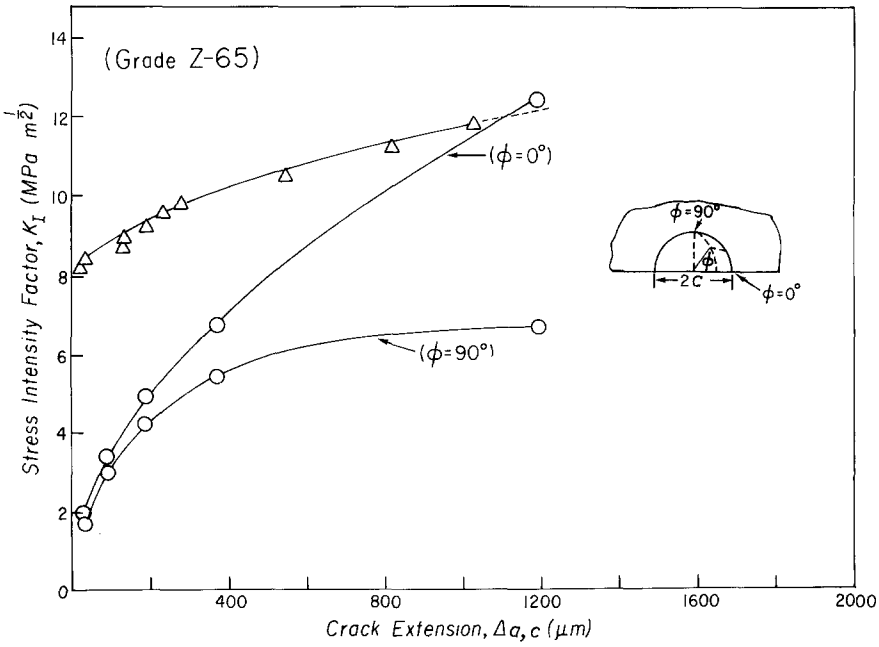

Figure 11 Comparison of the R-curve for CeO_2–TZP type IIA for a surface crack in (○) three-point-bend specimen with that obtained in (△) single-edge-notch-bend specimen: surface crack = c, edge crack = Δa.

beam specimen, particularly at small crack sizes. Similar differences have been observed in alumina [24] and MgO–PSZ [25]. The origin of the difference between the two R-curves in the case of the CeO_2–TZP is not completely clear. But there is an intrinsic difference in the relative scale and extent of the transformation zones in the two crack geometries. In the case of the single-edge-notch-beam specimen, the transformation zone is localized at the crack tip and the zone dimension is much smaller than the crack and specimen dimension. In the case of the surface crack, the crack nucleates and extends in an existing transformation band, in a manner analogous to nucleation of fatigue cracks in persistent slip bands in metals [26]. The crack-shielding effect of the transformation zones in the two crack geometries appears to be different.

5. Conclusions

1. Transformation yield stress of CeO_2–TZP measured in three-point bending increases systematically with decreasing grain size, consistent with the essential characteristics of stress-assisted transformation plasticity and the increased stability of the smaller grains.

2. The instantaneous nucleation and growth of the discrete, wedge-shaped transformation band in CeO_2–TZP suggests that transformation of grains is a cooperative phenomenon. A distinct yield stress, a yield stress plateau in strain and increasing band width and crack-tip zone sizes with decreasing yield stress are other important characteristics of transformation plasticity of CeO_2–TZP in three-point bending.

3. Significant differences in the crack-tip transformation zone sizes are observed in CeO_2–TZPs of varying yield stresses. However, R-curves measured for the different materials are not significantly different, thus suggesting that efficiency of crack-shielding apparently decreases with increasing zone size.

4. Crack-shielding models overestimate the fracture toughness increments for CeO_2–TZP based on the measured transformation zone widths. The discrepancy is greater for lower yield stress grades.

5. Dugdale's plastic strip zone model accounts properly for the transformation zone length as a function of the elastic stress-intensity factor. But the model needs further modification to account for the crack-growth-resistance behaviour.

6. R-curves estimated for surface cracks in the bend specimens differ significantly from the R-curve obtained in single-edge-notch-beam specimens, especially at small crack lengths. Differences are attributed to the different scale and extent of the transformation zones around the respective cracks and the different crack-shielding effects generated by them.

Acknowledgements

The paper is based on research supported by the Army Research Office under contract DAAL03-87-0060 at the University of Utah.

References

1. R. M. McMEEKING and A. G. EVANS, *J. Amer. Ceram. Soc.* **65** (1982) 242.
2. B. BUDIANSKY, J. W. HUTCHINSON and J. C. LAMBROPOULOS, *Int. J. Solids Structures* **19** (1983) 337.
3. J. C. LAMBROPOULOS, *J. Amer. Ceram. Soc.* **69** (1986) 218.
4. M. V. SWAIN and R. H. J. HANNINK, "R-Curve Behavior in Zirconia Ceramics", in "Science and Technology of Zirconia II", Advances in Ceramics, Vol. 12, edited by N. Claussen, M. Ruhle and A. H. Heuer (The American Ceramic Society, Westerville, Ohio, 1984) pp. 225–39.
5. D. B. MARSHALL and M. V. SWAIN, *J. Amer. Ceram. Soc.* **71** (1988) 399.
6. M. V. SWAIN, *Acta. Metall.* **33** (1985) 2083.
7. M. V. SWAIN and L. R. F. ROSE, *J. Amer. Ceram. Soc.* **69** (1986) 511.
8. R. C. GARVIE, R. H. J. HANNINK and M. V. SWAIN, *J. Mater. Sci. Lett.* **1** (1982) 437.
9. T. KOSMAC, R. WAGNER and N. CLAUSSEN, *J. Amer. Ceram. Soc.* **64** (1981) C-72.
10. C. S. YU and D. K. SHETTY, *ibid.* **72** (1989) 921.
11. L. R. F. ROSE and M. V. SWAIN, *Acta. Metall.* **36** (1988) 955.
12. H. TORAYA, M. YOSHIMURA and S. SOMIYA, *J. Amer. Ceram. Soc.* **71** (1988) 343.
13. MLD-STD-1942 (MR), "Flexural Strength of High Performance Ceramics at Ambient Temperature", November (1983).
14. ASTM E 399-83, "Standard Test Method for Plane Strain Fracture Toughness of Metallic Materials", Annual Book of ASTM Standards, Section 3, Vol. 03.01 (American Society for Testing and Materials, Philadelphia, 1984).
15. P. E. REYES-MOREL and I-WEI CHEN, *J. Amer. Ceram. Soc.* **71** (1988) 343.
16. D. S. DUGDALE, *J. Mech. Phys. Solids* **8** (1960) 100.
17. H. L. EWALDS and R. J. H. WANHILL, "Fracture Mechanics" (Edward Arnold, London, 1984) pp. 60–61.
18. G. T. HAHN and A. R. ROSENFIELD, *Acta Metall.* **13** (1965) 293.
19. A. H. HEUER, N. CLAUSSEN, W. M. KRIVEN and M. RUHLE, *J. Amer. Ceram. Soc.* **65** (1982) 642.
20. R. C. GARVIE and M. V. SWAIN, *J. Mater. Sci.* **20** (1985) 1193.
21. A. G. EVANS and R. M. CANNON, *Acta Metall.* **34** (1986) 761.
22 T. SAKUMA, Y. YOSHIZAWA and H. SUTO, *J. Mater. Sci.* **20** (1985) 2399.
23. J. C. NEWMAN Jr and I. S. RAJU, *Engng. Fract. Mech.* **15** (1981) 185.
24. R. W. STEINBRECH and O. SCHMENKEL, *J. Amer. Ceram. Soc.* **71** (1988) C-271.
25. D. B. MARSHALL and M. V. SWAIN, *J. Amer. Ceram. Soc.* **71** (1988) 399.
26. L. M. BROWN and S. L. OGIN, in "Fundamentals of Deformation and Fracture", The Eshelby Memorial Symposium, edited by B. A. Bilby, K. J. Miller and J. R. Willis (Cambridge University Press, 1985) pp. 501–29.

Received 16 January
and accepted 17 August 1989